Journal of CO_2 Utilization 9 (2015) 8–15

Contents lists available at ScienceDirect

Journal of CO_2 Utilization

journal homepage: www.elsevier.com/locate/jcou

CO_2 hydrogenation to methanol and dimethyl ether by Pd–Pd_2Ga catalysts supported over Ga_2O_3 polymorphs

Oscar Oyola-Rivera [a], Miguel Angel Baltanás [b], Nelson Cardona-Martínez [a,*]

[a] Department of Chemical Engineering, University of Puerto Rico–Mayagüez Campus, Mayagüez PR 00681-9000, Puerto Rico
[b] INTEC (Instituto de Desarrollo Tecnológico para la Industria Química, UNL/CONICET), Güemes 3450, S3000GLN Santa Fe, Argentina

ARTICLE INFO

Article history:
Received 13 June 2014
Received in revised form 15 September 2014
Accepted 3 November 2014
Available online

Keywords:
Pd_2Ga
Gallium oxide
CO_2 hydrogenation
Methanol
Dimethyl ether

ABSTRACT

The production of methanol and dimethyl ether (DME) *via* CO_2 hydrogenation was studied using Pd catalysts supported on α-Ga_2O_3, α-β-Ga_2O_3 and β-Ga_2O_3 polymorphs. The formation of a Pd_2Ga intermetallic compound was observed using XRD and XPS. The catalytic activity improves with an increase in the content of the Pd_2Ga intermetallic compound. The content of Pd_2Ga on Pd/Ga_2O_3 depends on the Ga_2O_3 crystalline phase of the catalyst. A slight catalytic deactivation was observed for all samples studied. The Pd/α-β-Ga_2O_3 catalyst displayed the largest deactivation. The deactivation appears to be caused by a loss of basic sites. The selectivity to dimethyl ether is not dependent on the Pd_2Ga content, but depends on the catalyst acidity. This assertion was tested by adding niobia to the catalysts, thus increasing the DME selectivity from 0 to 53%. The content of Pd_2Ga over Pd/Ga_2O_3 catalysts was identified to be a crucial parameter for CO_2 hydrogenation to methanol.

Published by Elsevier Ltd.

1. Introduction

Palladium supported over gallium oxide has become a prominent catalyst for steam reforming and dehydrogenation of methanol [1–5], dehydrogenation of ethanol [6] and carbon dioxide hydrogenation to methanol [7–10].

The gallium oxide polymorphism and stability was studied by Roy and co-workers in 1952 [11]. All gallia polymorphs can be converted to the β form at high temperatures, making this crystalline phase the only thermodynamically stable one. The β polymorph has a monoclinic structure [11–13], while the α polymorph has a hexagonal corundum structure [11,14].

Iwasa and co-workers observed the formation of an intermetallic compound between palladium and gallium for Pd/Ga_2O_3 catalysts that modified the catalytic properties of the material for steam reforming and dehydrogenation of methanol [2,3]. It was demonstrated that the formation and the ratio of Pd and Ga in this intermetallic compound depends on the reduction conditions [15,16]. The different Pd–Ga compounds exhibit similar orthorhombic structures, with the Pbnm space group [17–19].

Fujitani and co-workers were the first to report the use of a Pd–Ga_2O_3 based catalyst for the hydrogenation of CO_2 to methanol as an alternative to Cu/ZnO catalysts [10]. Baltanás and co-workers demonstrated that the deposition of Ga_2O_3 over Pd/SiO_2 catalysts significantly enhances the catalytic activity for CO_2 hydrogenation to methanol [20]. It was suggested that the hydrogenation intermediates involved in methanol synthesis from CO_2 are similar over Pd/Ga_2O_3 and Cu/ZnO [20–23]. On the other hand, Li and co-workers demonstrated that the formation of a Pd–Ga intermetallic compound over the Pd/Ga_2O_3 catalyst increases the catalytic performance for CO_2 hydrogenation to methanol [16].

A more detailed study of the CO_2 hydrogenation to methanol over Pd supported on different Ga_2O_3 polymorphs may yield a better understanding of the catalytic properties needed to promote this reaction. This work studies the role of Pd catalysts supported on Ga_2O_3 polymorphs for the catalytic conversion of CO_2 to methanol, focusing on characterization and CO_2 adsorption aspects.

2. Experimental

2.1. Materials

We used tetraammine palladium (II) nitrate solution (5.0 wt% as Pd) from Strem Chemicals as metal precursor, niobium (V)

* Corresponding author. Tel.: +1 787 832 4040x3747; fax: +1 787 265 3818.
E-mail addresses: tderliq@santafe-conicet.gov.ar (M.A. Baltanás), nelson.cardona@upr.edu (N. Cardona-Martínez).

http://dx.doi.org/10.1016/j.jcou.2014.11.003
2212-9820/Published by Elsevier Ltd.

chloride (99.99%) from Strem Chemicals as Nb_2O_5 precursor and gallium (III) nitrate hydrate 99.9998% from Acros Organics as the precursor for Ga_2O_3. A commercial catalyst support, Ga_2O_3 from Acros Organics, labeled LS-Ga_2O_3 due to its low surface area, was used as a comparison. Deionized (DI) water and 25% ammonium hydroxide in water from Acros Organics were used as solvents. For catalytic performance tests, the gases used include carbon dioxide (Food Grade, Praxair), hydrogen (High Purity, Praxair) and helium (High Purity, Praxair). Each gas was further purified with in-line VICI Metronics gas purifier traps. Nitrogen (Dry Grade, Praxair) was used as an internal standard for GC/MS analysis.

2.2. Catalysts preparation

The α, α-β and β Ga_2O_3 crystalline phases were synthesized using the procedure reported by Wang and co-workers [24]. Two main solutions were prepared in DI water, one with 10 wt% gallium precursor and another with 5 wt% ammonium hydroxide. These two solutions were mixed in a dropwise manner under vigorous stirring until the pH value reached approximately 9. The white precipitate was filtered, washed with distilled water, and dried at 353 K in air to obtain the Ga_2O_3 precursor. The precursor was calcined at 673 K for 5 h in air to obtain α-Ga_2O_3. The α-β-Ga_2O_3 and β-Ga_2O_3 samples were obtained by calcining α-Ga_2O_3 in air at 863 K and 1073 K, respectively. Catalysts with approximately 2 wt% loading were obtained by dispersing the Ga_2O_3 sample in an aqueous tetraammine palladium (II) nitrate solution, and heating at 343 K under constant stirring until the water was completely evaporated. The resulting powder was dried at 343 K in vacuum, followed by calcination at 673 K for 6 h. Finally, the sample was reduced at 573 K in flowing H_2 for 6 h.

Pd–Nb_2O_5/LS-Ga_2O_3 was prepared by the sequential impregnation of Pd nitrate and Nb chloride precursors on LS-Ga_2O_3 using evaporative deposition. The Pd precursor was first deposited on the support and the material was dried at 313 K for 24 h. Then the Nb precursor was deposited and the material was dried at 313 K. After the deposition of both precursors the material was calcined at 673 K in an air atmosphere, followed by H_2 reduction at 573 K for 6 h.

2.3. Catalysts characterization

The BET surface area was determined using an accelerated surface area and porosimetry system Micromeritics ASAP 2020 unit and nitrogen physisorption at liquid nitrogen temperature. The number of exposed Pd metal sites was estimated using hydrogen chemisorption at 308 K.

The crystal structure of the samples was determined using X-Ray diffraction with a Rigaku Ultima III X-Ray diffractometer equipped with cross beam optics and a Cu K_α target operating at 40 kV and 44 mA. Standard powder diffraction patterns were gathered for 2θ angles ranging from 20 to 80° at a scanning speed of 2°/min and a step size of 0.1°.

Galbraith Laboratories (Knoxville, TN) determined the loadings of palladium on the catalysts using ICP-AES. The samples were prepared using microwave assisted acid digestion at 453 K for at least 10 min.

The Pd and Pd_2Ga intermetallic compound content over the Ga_2O_3 polymorphs was determined using X-ray photoelectron spectroscopy data between 330 and 350 eV using a PHI VersaProbe 5000 Scanning X-ray Microprobe unit. The compositions were calculated based on the Pd $3d_{5/2}$ signals. All XP spectra were recorded with fixed analyzer transmission at room temperature, using monochromatic Al Kα radiation at pass energy of 187.85 eV leading to FWHM < 0.50 eV for the Ag $3d_{5/2}$ peak. Deconvolution of the spectra was conducted using the PHI MultiPak Software Version 9 with Gauss-Lorentz product functions after subtraction of a Shirley background.

For the determination of the isosteric heat of CO_2 adsorption, isotherms up to 0.11 MPa were measured at 308, 328 and 348 K, using the Micromeritics ASAP 2020 unit. Before the CO_2 uptakes were measured, each sample was pretreated at 543 K in H_2 for 2 h followed by evacuation.

We used infrared spectroscopy of adsorbed CO_2 and of adsorbed pyridine to study the basicity and acidity of our samples, respectively. In each case pressing about 50 mg of powder at 35 MPa metric tons made a self-supported 1 cm wafer. No phase transition for Ga_2O_3 is observed below 20,000 MPa [25]. For CO_2 adsorption experiments the disk was placed in the sample holder of a high-pressure transmission infrared stainless steel cell with water-cooled CaF_2 windows that was attached to a reactor flow system. The sample was pretreated by reduction *in situ* at 543 K in flowing 10% H_2 in N_2 (150 cm^3/min) for 2 h, followed by treatment in flowing N_2 (150 cm^3/min) at 543 K for 1 h to remove the gas phase H_2. After the reduction, the sample was cooled to room temperature and a spectrum of the clean surface taken. The CO_2 was adsorbed on the catalysts by flowing pure CO_2 (100 cm^3/min) over the samples at 308 K and 0.34 MPa for 1 h. After the adsorption period, the gas-phase CO_2 and any weakly adsorbed CO_2 were removed from the cell by flowing N_2 (100 cm^3/min) at 308 K until no CO_2 was detected in the outlet. Spectra were collected at room temperature in the absorbance mode using a Fourier Transform Infrared (FTIR) Spectrometer Thermo Scientific Nicolet 6700.

The characterization of the type of acid sites over the catalysts surface was performed using pyridine adsorption, in the same FTIR unit. In this instance the samples were first pretreated under hydrogen flow at 573 K, pressed and placed in the sample holder of a transmission infrared stainless steel cell with water-cooled CaF_2 windows. The sample disks were pretreated *in situ* at 623 K in flowing He (100 cm^3/min) for 1 h. After the activation, the sample was cooled to room temperature and a spectrum of the clean surface taken. Pyridine was adsorbed on the catalysts by passing a pyridine saturated helium stream through the cell at 473 K for 1 h at atmospheric pressure. The pyridine (E.M. Science, 99.92% purity) saturator was placed in a constant temperature bath kept at 273 K to produce a vapor pressure of about 640 Pa. After the adsorption period, the gas-phase pyridine and any weakly adsorbed pyridine were removed from the cell by flowing helium (100 cm^3/min) at 473 K overnight before cooling to room temperature and collecting a spectrum. Pyridine was desorbed sequentially by flowing He at 523, 573 and 623 K for 1 h at each temperature, followed by cooling to room temperature and taking a spectrum. The procedure for the identification of the acid types present is straightforward and has been described for samples equilibrated with a high pyridine pressure and subsequently evacuated at increasing temperatures [26]. The number of Lewis acid sites was estimated using the Beer–Lambert equation with the integrated molar extinction coefficients determined by Tamura and co-workers [27]. The molar extinction coefficient corresponding to Lewis acid sites at 1440 cm^{-1} was 1.73.

2.4. Catalytic performance

The catalytic performance for CO_2 hydrogenation was studied using a tubular fixed-bed reactor connected on-line to a GC/MS (HP 6890/HP 5973) and in-line to a CO_2 analyzer (Quantek Instruments Model 906). The reactor was packed with 0.5 g of catalyst with a particle diameter between 0.41 and 0.31 mm. The reactions were carried out at 543 K and 1.7 MPa with a H_2 to CO_2 ratio of 7.5. Before each reaction the catalyst was reduced *in situ* at 543 K and atmospheric pressure in flowing 10% H_2 in N_2 for 2 h.

Table 1
Catalysts characterization.

Catalyst	Metal wt%[a]	BET Surf. area (m^2/g)	Lewis sites (μmol/g)[b]	Metal sites (μmol/g)	Binding energy (eV)		Atomic %[c]		$q^{ads}_{CO_2}$ (kJ/mol)[d]
					Pd	Pd_2Ga	Pd	Pd_2Ga	
α-Ga_2O_3	–	62	2.4	–	–	–	–	–	–
α-β-Ga_2O_3	–	32	1.2	–	–	–	–	–	–
β-Ga_2O_3	–	28	2.0	–	–	–	–	–	–
Pd/α-Ga_2O_3	3.9	38	–	63	335.0	336.6	93.0	7.0	17.2
Pd/α-β-Ga_2O_3	2.2	38	–	67	335.6	336.8	77.0	23.0	21.6
Pd/β-Ga_2O_3	2.0	22	–	2	335.6	336.7	27.1	72.9	15.3
Pd/LS-Ga_2O_3	2.0	27	–	14	335.0	336.6	60.1	39.9	–

[a] As determined by Galbraith Laboratories using ICP.
[b] Lewis acid sites at reaction temperature estimated by interpolation of the number of acid sites after pyridine desorption at 523 and 573 K.
[c] XPS-measured Pd atomic percentages as metallic Pd or in Pd_2Ga, by deconvoluting the Pd 3d signals (see text).
[d] Isosteric heat of adsorption.

3. Results and discussion

3.1. Characterization

Table 1 shows the BET surface area of the Ga_2O_3 supported catalysts. The catalysts surface area decreases while the crystalline phase changes from α to β phase. This is the first signal of changes in structure. As shown in Fig. 1, XRD measurements confirmed the crystal structure changes. Fig. 1 displays the powder XRD patterns for the pure α and β phases of Ga_2O_3, as well as the XRD pattern for a polycrystalline structure of Ga_2O_3 containing mainly the α phase, together with a low concentration of the β phase. The low concentration of the β phase crystalline domains in the material is due to the calcination temperature used to generate the mixed structure (863 K), above which the β phase begins to form, as it was confirmed by Wang and co-workers [24]. The presence of the β phase is indicated by the appearance of a characteristic peak located at 30.5°, shown in the inset of Fig. 1, and a change in the relative intensities of the characteristic peaks of the α phase. The absence of the diffraction peaks at 31.5° and 35.5° that are characteristic for the β phase in the α-β-Ga_2O_3 sample is consistent with the (just) incipient formation of the β phase in the outer region of α-β-Ga_2O_3 as it was observed with UV Raman by Wang and co-workers [23]. The LS-Ga_2O_3 sample also featured the β phase.

The formation of intermetallic Pd_xGa species over Ga_2O_3 polymorphs occurs depending on the reduction temperature at which the Pd/Ga_2O_3 catalyst is exposed, and the crystalline phase of the Ga_2O_3 polymorph [1,15]. Lorenz and co-workers studied the formation of Pd_2Ga and PdGa under H_2 flow at temperatures between 373 K and 873 K on α-Ga_2O_3 and γ-Ga_2O_3 [1]. They observed that the fraction of Pd_2Ga on α-Ga_2O_3 and γ-Ga_2O_3 was close to one hundred percent by reducing at 523 K and 673 K under H_2 flow. On the other hand, Haghofer and co-workers studied the formation of Pd_2Ga and PdGa under H_2 flow at temperatures between 303 K and 773 K on β-Ga_2O_3 [15]. In this case, they observed the formation of Pd_2Ga at 673 K and PdGa at 773 K [15]. All catalysts reported in this study were reduced at 573 K in H_2 and then analyzed using XRD. In this study the only Pd_xGa species identified over the Ga_2O_3 polymorphs was Pd_2Ga.

The XRD patterns for the Pd impregnated Ga_2O_3 polymorphs are shown in Fig. 2. These XRD results are consistent with the formation of Pd_2Ga species on Pd/β-Ga_2O_3 and Pd/LS-Ga_2O_3, according to the work of Haghofer and co-workers [15]. The appearance of two characteristic peaks for Pd_2Ga at 39.6 and 40.3° for Pd/α-Ga_2O_3 and Pd/α-β-Ga_2O_3 also support the formation of Pd_2Ga over these materials. Moreover, a characteristic peak of α-Ga_2O_3 in the patterns of Pd/α-Ga_2O_3 and Pd/α-β-Ga_2O_3, overlapping the main characteristic peak of Pd_2Ga, increased its intensity after Pd deposition on these supports. Also an XRD peak at 44.7° in the Pd/α-Ga_2O_3 and Pd/α-β-Ga_2O_3 diffractograms is

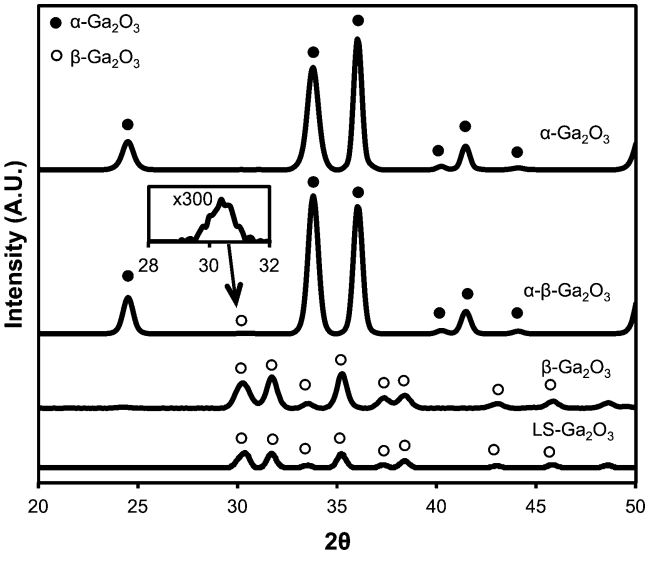

Fig. 1. Powder XRD patterns of the Ga_2O_3 polymorphs. The α-Ga_2O_3 sample was calcined in air at 673 K for 5 h. The α-β-Ga_2O_3 sample was first calcined in air at 673 K for 5 h followed by calcination at 873 K for 3 h. The β-Ga_2O_3 sample was first calcined in air at 673 K for 5 h followed by calcination at 1073 K for 3 h.

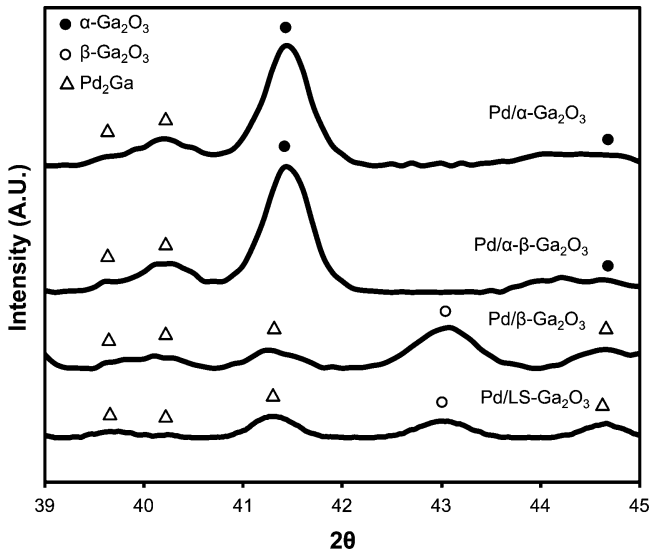

Fig. 2. Powder XRD patterns of the Pd/Ga_2O_3 catalysts following calcination in air at 673 K for 6 h and reduction in H_2 at 573 K for 6 h.

overlapped by a peak corresponding to the α-phase of both supports. These results are consistent with those obtained by Lorenz et al. [1], who observed the formation of Pd_2Ga over α-Ga_2O_3 at a similar reduction temperature.

The Pd_2Ga content on the catalysts surface was estimated by deconvoluting the XPS spectra of the samples. Fig. 3 shows the deconvoluted XPS spectra of Pd 3d core levels for the Pd supported on the Ga_2O_3 polymorphs and Table 1 summarizes the binding energies (BE). We did not find evidence for the formation of PdGa intermetallic species. The XPS spectra were deconvoluted using two spin-orbit doublets corresponding to metallic Pd with a Pd $3d_{5/2}$ BE signal of approximately 335.3 eV and the second corresponding to Pd_2Ga intermetallic compound with a Pd $3d_{5/2}$ BE signal of about 336.6 eV. The shift in BE from 335.3 eV to 336.6 eV is attributed to the formation of Pd_2Ga over the different Ga_2O_3 polymorphs [15]. Table 1 summarizes the atomic fraction of Pd present as metallic Pd and the atomic fraction present as Pd in Pd_2Ga (*i.e.*, the XPS-measured surface percentages) on the Ga_2O_3 polymorphs. The highest Pd_2Ga content was obtained for the samples containing the β-Ga_2O_3 crystalline phase, *i.e.*, Pd/β-Ga_2O_3 and Pd/LS-Ga_2O_3. The difference in Pd_2Ga abundance over the Ga_2O_3 polymorphs may depend on the Ga_2O_3 crystalline phase stability at 573 K under H_2, facilitating an induced reduction of the support by the spill of atomic hydrogen activated by Pd over the surface [16,28]. The low number of metals sites for Pd/β-Ga_2O_3 and Pd/LS-Ga_2O_3 determined using H_2 chemisorption is caused by a combination of higher Pd_2Ga content, lower Pd loading and lower surface area for these samples as shown in Table 1.

Fig. 4 shows FTIR spectra for pyridine adsorbed on the Ga_2O_3 polymorphs at 473 K normalized by the surface area of the sample. Only Lewis acidity is observed for the Ga_2O_3 supports, with characteristic bands between 1400 cm^{-1} and 1650 cm^{-1} [26]. When the spectra are normalized by the surface area of the samples the Lewis acidity at 473 K increases from α-Ga_2O_3 to β-Ga_2O_3 progressively. The effect of supporting Pd on the Ga_2O_3 polymorphs is shown in Fig. 5. The addition of the metal causes complex FTIR spectra for adsorbed pyridine with broad convolute bands near the bands observed for adsorption of pyridine on the supports. There is evidence from surface science studies under ultra high vacuum (UHV) conditions that pyridine has four main coordination modes when adsorbed to transition metal surfaces [29,30]. In one of those modes of adsorption, pyridine is dissociatively adsorbed with the formation of α-pyridyl species with both the nitrogen and α-carbon bonded to the surface. Under UHV conditions the formation of α-pyridyl species (C_5H_4N) at room temperature was observed on metal single crystals such as Cu(1 1 0) [31], Ni(1 0 0) [32], Pt(1 1 1) [29,31], Ru(0 0 1) [29,33] and W(1 1 0) [34]. For Pd(1 1 1) at 310 K pyridine adsorbs associatively to the surface predominately through the nitrogen lone pair [35]. On the other hand, Skotak and Karpiński observed H_2 evolution indicative of the formation

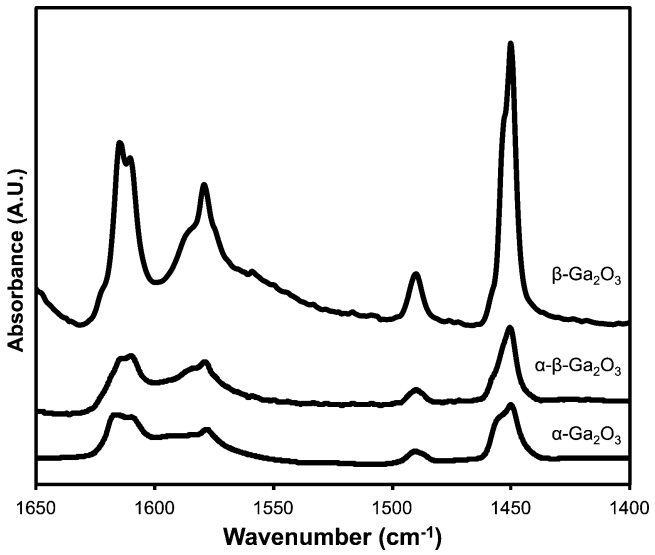

Fig. 4. Infrared spectra of pyridine adsorbed on the Ga_2O_3 polymorphs at 473 K normalized by the surface area of the sample.

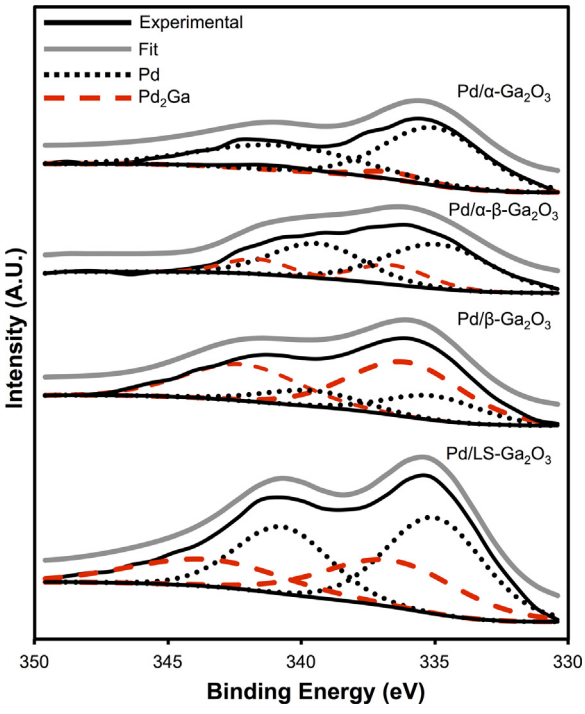

Fig. 3. XPS spectra (Pd 3d signals) for the supported Pd/Ga_2O_3 catalysts following calcination in air at 673 K for 6 h and reduction in H_2 at 573 K for 6 h. For clarity the fit line was displaced from the experimental line by 500 A.U.

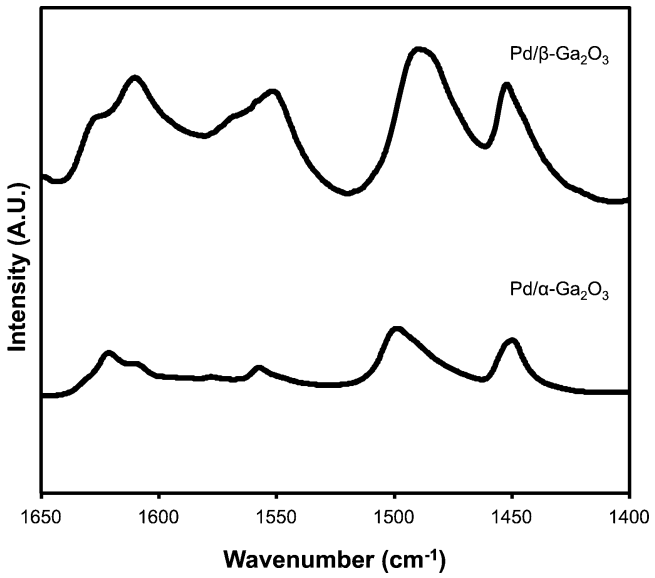

Fig. 5. Infrared spectra of pyridine adsorbed on Pd/Ga_2O_3 catalysts at 473 K normalized by the surface area of the sample.

of α-pyridyl species during pyridine TPD from Pd/Al_2O_3 starting at around 393–423 K depending on the Pd loading [36]. Based on surface science results for pyridine adsorbed on Pt(1 1 1) and W(1 1 0), Shen and coworkers assigned new bands observed after the adsorption of pyridine on Ni/Al_2O_3 around 1553, 1416 and 1393 cm^{-1} to the α-pyridyl species adsorbed on Ni [37]. These authors also assigned bands at around 1600, 1489 and 1443 cm^{-1} to molecular pyridine adsorbed on Ni [37]. From the previous discussion it is clear that pyridine adsorption on metals supported on metal oxides is difficult to interpret due to the overlapping of bands for the adsorbed pyridine on the support and supported metal and the formation of α-pyridyl species on the metal that also give bands that overlap with bands for pyridine adsorbed on the support. The overlapping bands lead to difficult assignments of spectral bands. Deconvolution of the spectra in Fig. 5 reveals the appearance of strong absorption bands located at 1551 to 1557 cm^{-1}, corresponding to the formation of α-pyridyl species adsorbed on Pd, and at 1591 to 1593 cm^{-1} that we believe correspond to pyridine molecularly adsorbed on Pd.

Since pyridine is not a good test molecule to study the acidity of Pd catalysts supported on Ga_2O_3, the relationship between the catalyst acidity and selectivity to DME was compared using the acidity determined for the Ga_2O_3 supports. The number of acid sites were estimated using the Beer–Lambert equation based on the pyridine remaining on the surface after desorption at temperatures between 473 and 623 K. As observed in Fig. 6, on a mass basis the number of Lewis acid sites decreases monotonically with an increase in the desorption temperature. This reduction in the number of acid sites with the increase in the desorption temperature of pyridine is related to the relative acid strength [38]. The decrease in acidity with the increase in temperature is higher for β-Ga_2O_3 than for the other Ga_2O_3 samples. Thus, the reduction in acidity for β-Ga_2O_3 may be attributed to a weaker acid strength compared with the other supports. The acidity on β-Ga_2O_3 is reduced from 2.6 to approximately 2.0 μmol/g, thus having less acid sites than α-Ga_2O_3 but having more acid sites than α-β-Ga_2O_3 at the reaction temperature (543 K).

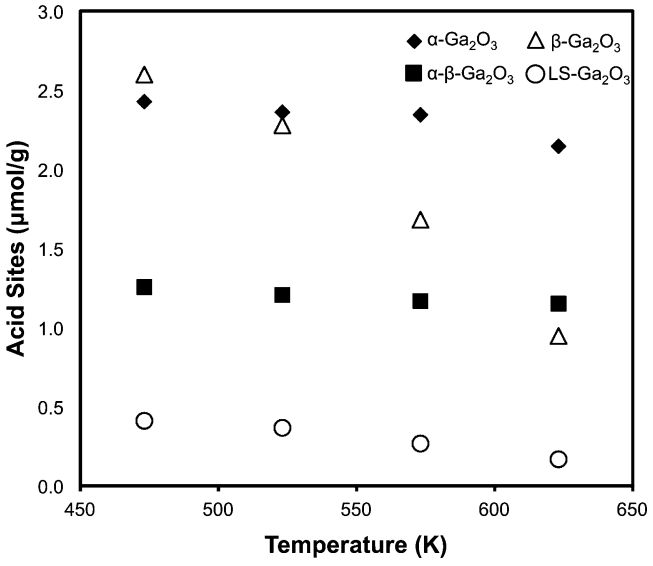

Fig. 6. Number of Lewis acid sites on the Ga_2O_3 supports as a function of pyridine desorption temperature. The number of acid sites were estimated using the Beer–Lambert equation based on the pyridine remaining on the surface after desorption at temperatures between 473 and 623 K.

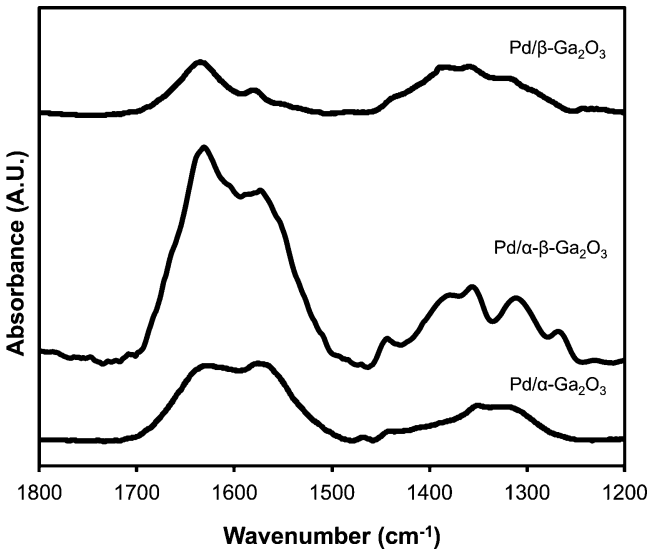

Fig. 7. Infrared spectra of CO_2 adsorbed on Pd/Ga_2O_3 catalysts at 308 K and 0.34 MPa.

3.2. CO_2 adsorption

FTIR spectra after CO_2 adsorption for Pd supported over Ga_2O_3 polymorphs were collected at 308 K and 0.34 MPa in a N_2 atmosphere, as shown in Fig. 7. Two characteristic bands at 1630 and 1580 cm^{-1}, which are observed for all samples, correspond to two low strength basic sites. The band at 1630 cm^{-1} corresponds to CO_2 bonded as bicarbonate and the band at 1580 cm^{-1} corresponds to CO_2 bonded as a bidentate carbonate on the catalyst surface [39,40]. The CO_2 adsorption properties change depending on the Ga_2O_3 polymorph present and the ratio of the peak area for bidentate carbonate and bicarbonate bands changes between phases. The bicarbonate to bidentate carbonate ratio of the IR peak areas for these bands are 1.0, 1.3 and 3.5 for Pd supported on α-Ga_2O_3, α-β-Ga_2O_3 and β-Ga_2O_3, respectively. Hence, the content of bicarbonate species is higher for Pd supported on β-Ga_2O_3. The bicarbonates require surface hydroxyl groups that are considered weak base sites whereas bidentate carbonates require the participation of an adjacent cationic site that are medium-strength basic sites [40,41]. These carbonate species induce the formation of formate species in the presence of H_2 on the catalysts surface [42–44]. The formate species are intermediates for CO_2 hydrogenation and were previously identified as possible precursors for the formation of methoxy groups for methanol synthesis [42–44].

FTIR spectra for CO_2 adsorption over α-Ga_2O_3 at temperatures from 323 to 473 K were collected, as shown in Fig. 8. The abovementioned bands decreased in intensity with increasing temperature confirming a moderate interaction between the CO_2 molecule and the Ga_2O_3 basic sites, in agreement with the work of Collins et al. [39].

The isosteric heat of adsorption, $q^{ads}_{CO_2} = -\Delta H^{ads}_{CO_2}$, was calculated using the Clausius Clapeyron equation from adsorption data from 308 to 348 K for the Pd supported catalysts over the Ga_2O_3 polymorphs, as shown in Table 1. The isosteric heat seems to be influenced by the Ga_2O_3 crystalline phase. The isosteric heats of adsorption for the samples with predominantly the alpha phase display a slightly larger value than the ones associated with the beta phase.

3.3. Catalytic performance

The main reaction product for CO_2 hydrogenation on Pd/Ga_2O_3 at 543 K and 1.72 MPa is methanol. Dimethyl ether (DME) is also

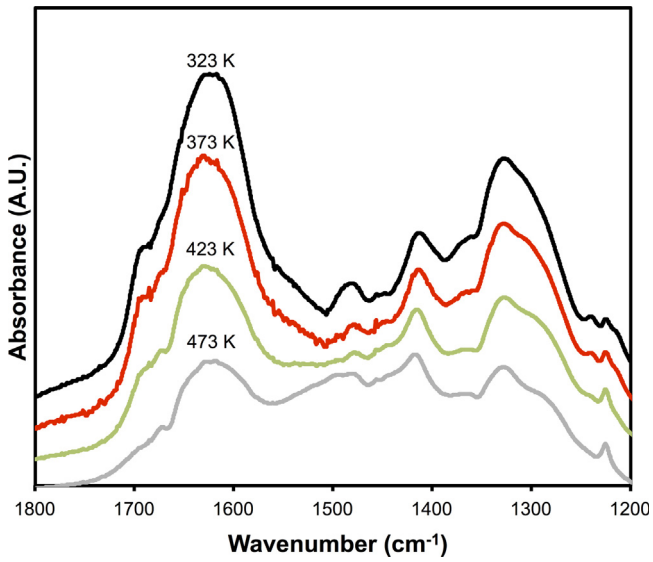

Fig. 8. Infrared spectra of CO_2 adsorbed on α-Ga_2O_3 at 323 K and atmospheric pressure followed by desorption at 373, 423 and 473 K in flowing He (100 cm^3 min^{-1}).

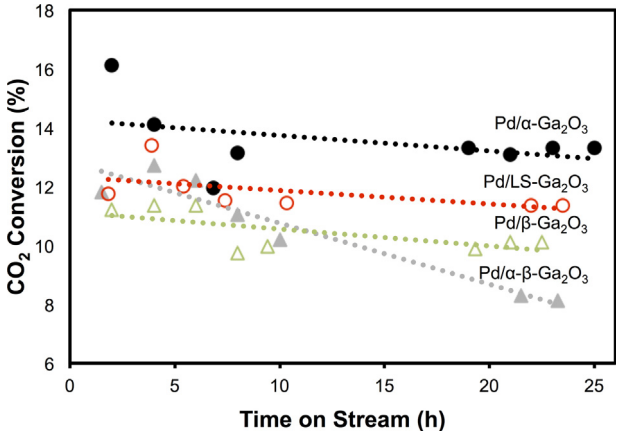

Fig. 9. Effect of time on stream on CO_2 conversion for Pd catalysts supported on Ga_2O_3 polymorphs at 543 K, 1.72 MPa and WHSV = 27 h^{-1}.

observed as a result of methanol dehydration on the acid sites of Ga_2O_3 [45–47]. The turnover frequency (TOF) was estimated using the initial CO_2 conversion and the exposed Pd metal sites (pure Pd) as determined by H_2 chemisorption. A control experiment using the β-Ga_2O_3 support did not display measurable activity for CO_2 hydrogenation.

Table 2 allows comparing the reaction results for the complete set of Pd catalysts supported on the Ga_2O_3 polymorphs. The TOF changes with a change in the Ga_2O_3 crystal phase and increases with an increment in the Pd_2Ga content present on the catalyst surface. Based on the observed catalytic performances, the catalyst prepared with the β-Ga_2O_3 crystal phase, featuring the highest content of Pd_2Ga (and, thence, the lowest amount of metallic Pd) showed the highest TOF. Yet, it is not entirely obvious whether the increase of the Pd_2Ga content over the surface improved the catalysts activity, because the CO_2 conversion was (somewhat) higher on Pd/α-Ga_2O_3 than on Pd/α-β-Ga_2O_3 or Pd/β-Ga_2O_3. The first two catalysts had about the same surface area and Pd_2Ga surface percentage, but the Pd/α-Ga_2O_3 had a higher loading of Pd. Rather, it is highly likely that the metallic function in all these catalysts is sufficient for supplying atomic hydrogen, while the oxidic surface of the different gallia polymorphs (where the actual, progressive hydrogenation of the chemisorbed carbonaceous intermediates proceeds [48]) deserves special attention or scrutiny.

Table 2
Catalytic performance for CO_2 hydrogenation at pseudo-steady state on Pd/Ga_2O_3, Pd/LS-Ga_2O_3 and Pd–Nb_2O_5/LS-Ga_2O_3.[a]

Catalyst	X_{CO2} (%)	TOF (s^{-1})	DME selectivity (%)
Pd/α-Ga_2O_3	14	0.27	22
Pd/α-β-Ga_2O_3	12	0.23	12
Pd/β-Ga_2O_3	12	8.8	13
Pd/LS-Ga_2O_3	12	1.1	4
	6[b]	0.9	0
Pd–Nb_2O_5/LS-Ga_2O_3[c]	5	1.5	53

[a] Reaction conditions: P = 1.7 MPa, T = 543 K, molar H_2:CO_2 = 7.5, WHSV = 27 h^{-1}.
[b] Molar H_2:CO_2 = 6.4, WHSV = 44 h^{-1}.
[c] Pd loading = 2 wt%, Surface area = 19 m^2 g^{-1}, exposed metal sites = 4 μmol g^{-1}.

As mentioned above, the ratio of bicarbonate to bidentate carbonate species adsorbed on the Ga_2O_3 surface changed with a change in the Ga_2O_3 crystal phase and a higher ratio between these species was observed for Pd supported on the β-Ga_2O_3 polymorph. The highest TOF corresponded to the highest ratio of bicarbonate to bidentate carbonate observed. This finding suggests that the increase in the activity for CO_2 hydrogenation may be promoted by an adequate formation of bicarbonate species on the gallia surface.

An analysis of the change in conversion of CO_2 as a function of time on stream (TOS) indicates that there was some deactivation in all the materials studied, as shown in Fig. 9. Pd/α-β-Ga_2O_3 had the highest deactivation with TOS. This catalyst had the lowest Pd_2Ga content as well. This observation suggested us that α-β-Ga_2O_3 might be less stable than the other polymorphs under the experimental conditions used. Thus, the decrease in CO_2 conversion might be attributed to the catalyst deactivation caused by a reduction of the number of basic active sites on the Ga_2O_3 polymorphs [49]. The reduction of basic sites over α-β-Ga_2O_3 was confirmed by comparing the CO_2 adsorption isotherms of Pd/α-β-Ga_2O_3 before and after reaction, as shown in Fig. 10. The CO_2 uptake for Pd/α-β-Ga_2O_3 decreased to about 52% of the original value at 0.1 MPa equilibrium pressure. One possible explanation may be that exposure to high concentrations of H_2 at high temperature during the reaction can cause a partial reduction of

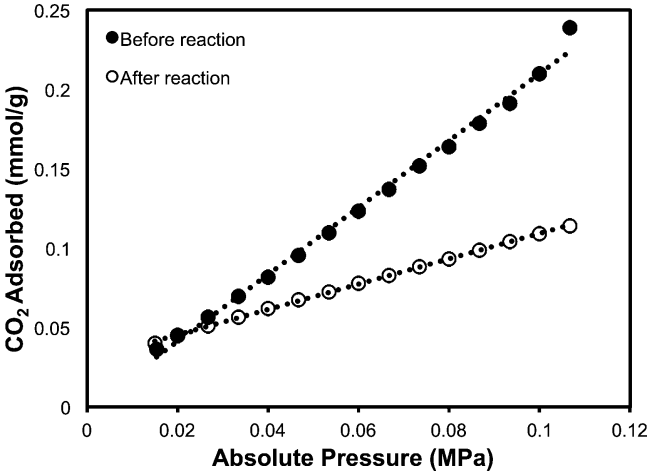

Fig. 10. CO_2 adsorption isotherms for fresh and deactivated Pd/α-β-Ga_2O_3 at 308 K. The samples were degassed at 423 K for 6 h before adsorption.

Ga_2O_3 that in turn can cause a decrease in the number of basic sites on the surface by the loss of oxygen in the structure. Therefore, it could be that catalyst deactivation is due to a higher loss of basic sites in α-β-Ga_2O_3, by the progressive superficial reduction of Ga_2O_3, than on the other – more stable- polymorphs.

Table 2 shows the selectivity to DME of the Pd/Ga_2O_3 catalysts at similar conversions (12–14%). The highest selectivity to DME was obtained over Pd/α-Ga_2O_3. Several reaction mechanisms for methanol conversion to DME have been proposed. While some works have attributed said conversion to the dehydration of methanol to DME on Brønsted sites, others ascribed it to Lewis sites [46,50–53]. The acidity results presented in Section 3.1 for Pd/Ga_2O_3 do not allow to ascertain whether Brønsted or Lewis sites favor the dehydration of methanol to DME. On the other hand, the selectivity to DME over Pd/Ga_2O_3 catalysts can be related to the acidity of Ga_2O_3 polymorphs supports. The supports only display Lewis acidity. The DME selectivity increases as the number of acid sites increases on Ga_2O_3 supports at the reaction temperature. Therefore, these results suggest that the DME selectivity over Pd/Ga_2O_3 catalysts depends on the number of Lewis acid sites for these catalysts.

As mentioned above, DME is produced from the dehydration of methanol as a result of the acidity of Ga_2O_3, which is rather moderate. Based on this, niobium oxide (Nb_2O_5) was added to the Pd/LS-Ga_2O_3 catalyst surface in an attempt to increase the selectivity to DME of the catalyst, as Nb_2O_5 is often used in dehydration reactions due to its high acidity [54–57]. Adding niobia to the Pd/LS-Ga_2O_3 catalyst caused a 30% loss in surface area. However, for similar pseudo-steady state conversions of CO_2 (5–6% obtained by changing the WHSV) the TOF almost doubled upon addition of Nb_2O_5, and the DME selectivity increased dramatically for Pd–Nb_2O_5/LS-Ga_2O_3, up to 53% from mere traces on Pd/LS-Ga_2O_3. Thus, this demonstrates that the selectivity to DME can be enhanced by the addition of strong acidic species on the catalyst surface.

Fig. 11 shows the change in selectivity to methanol and DME over time on stream (TOS) for the Pd–Nb_2O_5/LS-Ga_2O_3 catalyst. The first product that was observed was DME and was the only product observed for 8 h of TOS. Methanol was first observed after 9 h TOS. The selectivity to DME gradually decreased, from 100% to 53%, between the 10 and 20 h on stream and remained nearly constant thereafter. Noteworthy, in this experiment no reaction products were observed until after 1 h on stream, which suggests that the preparation method (subsequent deposition of niobia onto the Pd/LS-Ga_2O_3 catalyst might have caused an occlusion of the palladium

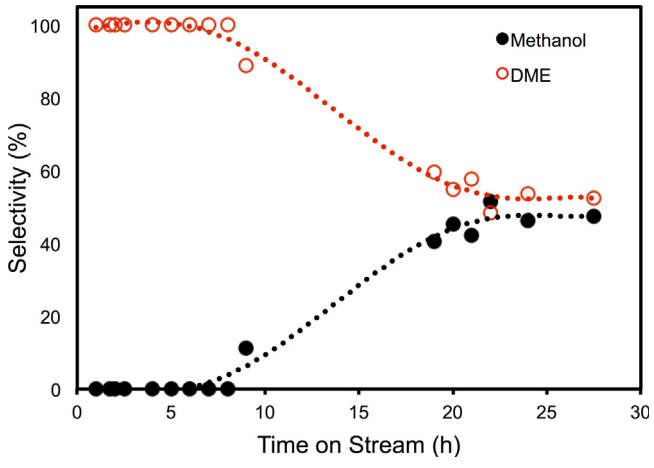

Fig. 11. Effect of time on stream on methanol and DME selectivity for Pd–Nb_2O_5/LS-Ga_2O_3 at 543 K, 1.72 MPa and WHSV = 27 h^{-1}.

crystallites and/or a combination with the niobia (that merits to be explored further indeed) which progressively gave way to exposed, free metal–or intermetallic-particles with TOS. Nonetheless, these results show that the selectivity to DME can be enhanced by the addition of Nb_2O_5 onto the surface and that increase remains constant once the steady state is reached.

4. Conclusions

The catalytic activity of Pd supported over Ga_2O_3 seems to be related to the formation and content of the intermetallic compound Pd_2Ga. The Pd_2Ga content varies depending on the Ga_2O_3 polymorphs. The catalytic activity is also a function of the CO_2 adsorption properties on the different Ga_2O_3 polymorphs, specifically by the formation of bicarbonate as a precursor of formate species. The reduction of the number of basic sites on Ga_2O_3 during the reaction appears to cause catalyst deactivation. The catalysts selectivity depends on the acidity of the gallia; the increment in the number of acid sites increases the conversion of methanol and DME. Thus, both the formation of the intermetallic compound Pd_2Ga and the type of Ga_2O_3 polymorph have a strong impact on the catalytic hydrogenation of CO_2. The addition of a strong acid, Nb_2O_5, to Pd/LS-Ga_2O_3 was also evaluated for the increase in selectivity towards DME. Under the same experimental conditions, our results confirm that the addition of niobia to the catalyst surface increases the selectivity to DME substantially.

Acknowledgments

This work was supported through the NSF PREM: Wisconsin-Puerto Rico Partnership for Research and Education in Materials (Award DMR-0934115). We wish to also acknowledge partial support from the NSF funded Puerto Rico Institute for Functional Nanomaterials (Award EPS-1002410). Technical support of Mr. Angel Zapata-Alma, Prof. Arturo Hernández-Maldonado and Prof. María Martínez-Iñesta is appreciated. MAB thanks CONICET and UNL for their continued support.

References

[1] H. Lorenz, R. Thalinger, E.-M. Köck, M. Kogler, L. Mayr, D. Schmidmair, T. Bielz, K. Pfaller, B. Klötzer, S. Penner, Appl. Catal. A: Gen. 453 (2013) 34–44.
[2] N. Iwasa, T. Mayanagi, N. Ogawa, K. Sakata, N. Takezawa, Catal. Lett. 54 (1998) 119–123.
[3] N. Iwasa, N. Takezawa, Top. Catal. 22 (2003) 215–224.
[4] N. Iwasa, W. Nomura, T. Mayanagi, S. Fujita, M. Arai, N. Takezawa, J. Chem. Eng. Jpn. 37 (2004) 286–293.
[5] S.E. Collins, M.A. Baltanás, A.L. Bonivardi, Appl. Catal. A: Gen. 295 (2005) 126–133.
[6] N. Iwasa, O. Yamamoto, R. Tamura, M. Nishikubo, N. Takezawa, Catal. Lett. 62 (1999) 179–184.
[7] N. Iwasa, H. Suzuki, M. Terashita, M. Arai, N. Takezawa, Catal. Lett. 96 (2004) 75–78.
[8] S.E. Collins, D.L. Chiavassa, A.L. Bonivardi, M.A. Baltanás, Catal. Lett. 103 (2005) 83–88.
[9] T. Fujitani, I. Nakamura, Bull. Chem. Soc. Jpn. 75 (2002) 1393–1398.
[10] T. Fujitani, M. Saito, Y. Kanai, T. Watanabe, J. Nakamura, T. Uchijima, Appl. Catal. A: Gen. 125 (1995) L199–L202.
[11] R. Roy, V.G. Hill, E.F. Osborn, J. Am. Chem. Soc. 74 (1952) 719–722.
[12] J. Åhman, G. Svensson, J. Albertsson, Acta Crystallogr. Sect. C: Cryst. Struct. Commun. 52 (1996) 1336–1338.
[13] S. Geller, J. Chem. Phys. 33 (1960) 676.
[14] M. Marezio, J.P. Remeika, J. Chem. Phys. 46 (1967) 1862–1865.
[15] A. Haghofer, K. Föttinger, F. Girgsdies, D. Teschner, A. Knop-Gericke, R. Schlögl, G. Rupprechter, J. Catal. 286 (2012) 13–21.
[16] L. Li, B. Zhang, E. Kunkes, K. Föttinger, M. Armbrüster, D.S. Su, W. Wei, R. Schlögl, M. Behrens, ChemCatChem 4 (2012) 1764–1775.
[17] M.K. Bhargava, A.A. Gadalla, K. Schubert, J. Less-Common Met. 42 (1975) 69–76.
[18] K. Khalaff, K. Schubert, J. Less-Common Met. 37 (1974) 129–140.
[19] S. Penner, H. Lorenz, W. Jochum, M. Stöger-Pollach, D. Wang, C. Rameshan, B. Klötzer, Appl. Catal. A: Gen. 358 (2009) 193–202.
[20] A.L. Bonivardi, D.L. Chiavassa, C.A. Querini, M.A. Baltanás, in: A. Corma, F.V. Melo, S. Mendioroz, J.L.G. Fierro (Eds.), Stud. Surf. Sci. Catal., Elsevier, Amsterdam, 2000, pp. 3747–3752.

[21] H. Arakawa, in: T. Inui, M. Anpo, K. Izui, S. Yanagida, T. Yamaguchi (Eds.), Stud. Surf. Sci. Catal., Elsevier, Amsterdam, The Netherlands, 1998, pp. 19–30.
[22] G. Millar, C.H. Rochester, K. Waugh, Catal. Lett. 14 (1992) 289–295.
[23] S.-i. Fujita, M. Usui, E. Ohara, N. Takezawa, Catal. Lett. 13 (1992) 349–358.
[24] X. Wang, Q. Xu, M. Li, S. Shen, X. Wang, Y. Wang, Z. Feng, J. Shi, H. Han, C. Li, Angew. Chem. Int. Ed. 51 (2012) 13089–13092.
[25] D. Machon, P.F. McMillan, B. Xu, J. Dong, Phys. Rev. B 73 (2006) 094125.
[26] N. Cardona-Martínez, J.A. Dumesic, J. Catal. 125 (1990) 427–444.
[27] M. Tamura, K.-i. Shimizu, A. Satsuma, Appl. Catal. A: Gen. 433–434 (2012) 135–145.
[28] S. Penner, B. Jenewein, K. Hayek, Catal. Lett. 113 (2007) 65–72.
[29] M.E. Bridge, M. Connolly, D.R. Lloyd, J. Somers, P. Jakob, D. Menzel, Spectrochim. Acta A: Mol. Biomol. Spectrosc. 43 (1987) 1473–1478.
[30] M.R. Cohen, R.P. Merrill, Surf. Sci. 245 (1991) 1–11.
[31] S. Haq, D.A. King, J. Phys. Chem. 100 (1996) 16957–16965.
[32] N.J. DiNardo, P. Avouris, J.E. Demuth, J. Chem. Phys. 81 (1984) 2169–2180.
[33] P. Jakob, D.R. Lloyd, D. Menzel, Surf. Sci. 227 (1990) 325–336.
[34] M.P. Andersson, P. Uvdal, J. Phys. Chem. B 105 (2001) 9458–9462.
[35] V.H. Grassian, E.L. Muetterties, J. Phys. Chem. 91 (1987) 389–396.
[36] M. Skotak, Z. Karpiński, Chem. Eng. J. 90 (2002) 89–96.
[37] J. Zhao, H. Chen, J. Xu, J. Shen, J. Phys. Chem. C 117 (2013) 10573–10580.
[38] F.A. Diaz-Mendoza, L. Pernett-Bolano, N. Cardona-Martínez, Thermochim. Acta 312 (1998) 47–61.
[39] S.E. Collins, M.A. Baltanás, A.L. Bonivardi, J. Phys. Chem. B 110 (2006) 5498–5507.
[40] Q. Liu, L. Wang, C. Wang, W. Qu, Z. Tian, H. Ma, D. Wang, B. Wang, Z. Xu, Appl. Catal. B: Environ. 136–137 (2013) 210–217.
[41] M. León, E. Díaz, S. Bennici, A. Vega, S. Ordóñez, A. Auroux, Ind. Eng. Chem. Res. 49 (2010) 3663–3671.
[42] J. Weigel, R.A. Koeppel, A. Baiker, A. Wokaun, Langmuir 12 (1996) 5319–5329.
[43] Y. Yang, J. Evans, J.A. Rodriguez, M.G. White, P. Liu, Phys. Chem. Chem. Phys. 12 (2010) 9909–9917.
[44] S.E. Collins, M.A. Baltanás, A.L. Bonivardi, J. Catal. 226 (2004) 410–421.
[45] F. Yaripour, F. Baghaei, I. Schmidt, J. Perregaard, Catal. Commun. 6 (2005) 147–152.
[46] M. Xu, J.H. Lunsford, D.W. Goodman, A. Bhattacharyya, Appl. Catal. A: Gen. 149 (1997) 289–301.
[47] C.D. Chang, A.J. Silvestri, J. Catal. 47 (1977) 249–259.
[48] D.L. Chiavassa, S.E. Collins, A.L. Bonivardi, M.A. Baltanás, Chem. Eng. J. 150 (2009) 204–212.
[49] P. Michorczyk, J. Ogonowski, React. Kinet. Catal. Lett. 78 (2003) 41–47.
[50] M.B. Sayed, R.A. Kydd, R.P. Cooney, J. Catal. 88 (1984) 137–149.
[51] H. Knözinger, R. Köhne, J. Catal. 3 (1964) 559–560.
[52] H. Knözinger, K. Kochloefl, W. Meye, J. Catal. 28 (1973) 69–75.
[53] E. Lalik, X. Liu, J. Klinowski, J. Phys. Chem. 96 (1992) 805–809.
[54] J. Datka, A.M. Turek, J.M. Jehng, I.E. Wachs, J. Catal. 135 (1992) 186–199.
[55] K. Tanabe, Catal. Today 78 (2003) 65–77.
[56] J.-M. Jehng, I.E. Wachs, Catal. Today 8 (1990) 37–55.
[57] K. Tanabe, S. Okazaki, Appl. Catal. A: Gen. 133 (1995) 191–218.